

ARTICLE OPEN ACCESS

A Patient-Derived 3D Cyst Model of Polycystic Kidney Disease That Mimics Disease Development and Responds to Repurposing Candidates

Alina Meyer¹  | Bola Khalil^{2,3}  | Margarita Iljin⁴  | Hester Bange⁴ | Leo S. Price⁴  | Natalia Dyubankova²  | Gerard J. P. van Westen³  | Herman van Vlijmen²  | Dorien J. M. Peters⁵  | Per Artursson¹ 

¹Department of Pharmacy, Uppsala University, Uppsala, Sweden | ²In Silico Discovery, J&J Innovative Medicine, Beerse, Belgium | ³Division of Medicinal Chemistry, Leiden Academic Centre for Drug Research, Leiden, the Netherlands | ⁴Crown Bioscience Netherlands B.V, Leiden, the Netherlands | ⁵Department of Human Genetics, Leiden University Medical Center, Leiden, the Netherlands

Correspondence: Per Artursson (per.artursson@uu.se)

Received: 30 October 2024 | **Revised:** 22 February 2025 | **Accepted:** 14 March 2025

Funding: The study was supported by the European Union's Horizon 2020 research and innovation programme under the Marie Skłodowska Curie grant agreement No. 955879 (DRUGtrain). This work was supported by the Swedish Research Council grant (number 1951) for Per Artursson.

Keywords: 3D cyst cultures | ADPKD | global proteomics | human | kidney

ABSTRACT

Autosomal dominant polycystic kidney disease (ADPKD) is the most common hereditary kidney disease. Its progressively expanding, fluid-filled renal cysts eventually lead to end-stage renal disease. Despite the relatively high prevalence, treatment options are currently limited to a single drug approved by the FDA and EMA. Here, we investigated human ADPKD patient-derived three-dimensional cyst cultures (3DCC) as an *in vitro* model for ADPKD and drug repurposing research. First, we analyzed the proteomes of 3DCC derived from healthy and diseased tissues. We then compared the protein expression profiles with those of reference tissues, mainly from the same patients. We quantified 290 proteins affecting drug disposition and proposed target proteins for drug treatment. Lastly, we investigated the functional response of the quantified target proteins after exposure to repurposing candidates in the 3DCC. Proteomic profiling of human 3DCC reflected previously reported pathophysiological alterations, including aberrant protein expression in inflammation and metabolic reprogramming. While the 3DCCs largely recapitulated the disease phenotype *in vitro*, drug transporter expression was reduced compared to *in vivo* conditions. Target proteins for proposed repurposing candidates showed similar expression *in vitro* and in tissues. Exposure to these repurposing candidates inhibited cyst swelling *in vitro*, supporting the suitability of the 3DCC for ADPKD drug screening. In summary, our results provide new insights into the ADPKD proteome and offer a starting point for further research to improve treatment options for affected individuals.

1 | Introduction

Autosomal dominant polycystic kidney disease (ADPKD) is a chronic, progressive, hereditary disease with a prevalence of 4

to 10/10,000. ADPKD mainly manifests as fluid-filled cysts in the kidney, liver, and other organs, which increase in number and size over time and eventually lead to end-stage renal disease. Common symptoms include pain, bleeding, infections,

The Work Has Previously Been Presented at the Following Meetings: Proteomics in cell biology and disease mechanisms conference, Heidelberg, Germany (25–27 Oct 2023). ISSX Workshop on Quantitative LC–MS/MS Proteomics, Sheffield, United Kingdom (27–28 Jun 2024). 2024 ISSX/ISSX Meeting, Honolulu, United States of America (15–18 Sep 2024). HUPO 2024, Dresden, Germany (20–23 Oct 2024).

This is an open access article under the terms of the [Creative Commons Attribution-NonCommercial](https://creativecommons.org/licenses/by-nc/4.0/) License, which permits use, distribution and reproduction in any medium, provided the original work is properly cited and is not used for commercial purposes.

© 2025 The Author(s). *Clinical and Translational Science* published by Wiley Periodicals LLC on behalf of American Society for Clinical Pharmacology and Therapeutics.

Summary

- What is the current knowledge on the topic?
 - Despite significant advances in proteomic analysis of ADPKD, much of the research has been limited to non-human models and human urinary extracellular vesicles.
 - This leaves a significant gap in our understanding of how global protein expression in human 3D in vitro systems aligns with actual patient kidney tissues.
 - Furthermore, the translation of these protein expression patterns into phenotypic responses has yet to be investigated.
- What question did this study address?
 - Our study offers a comprehensive analysis of the proteome of human 3D cyst cultures from healthy and late-stage ADPKD patients, additionally comparing them with corresponding reference tissues.
 - We investigate how accurately these in vitro models reflect the protein expression patterns found in ADPKD tissues.
 - Additionally, we examine the correlation between drug target protein expression and functional cyst swelling responses, showcasing the potential of our 3D cyst cultures for effective ADPKD drug screening.
- What does this study add to our knowledge?
 - Our comprehensive protein expression analysis uncovers that key disease pathways—such as inflammation and metabolic reprogramming—are accurately represented in the 3D in vitro model.
 - Most of the drug targets we examined are expressed in the 3D cyst cultures, and their functional responses to repurposing candidates highlight the model's potential for advancing translational drug discovery and development in ADPKD.
- How might this change clinical pharmacology or translational science?
 - This study provides comprehensive insights into the differential protein expression between healthy individuals and ADPKD patients, setting the stage for biomarker and drug target discovery.
 - Moreover, our detailed characterization of the 3D in vitro model opens up for high-quality drug screenings, potentially accelerating the identification of novel treatments for ADPKD.

hypertension, and cardiovascular diseases [5]. ADPKD is genetically heterogeneous but is most commonly caused by mutations in the *PKD1* (approx. 78% of cases) or *PKD2* (approx. 15% of cases) genes, which encode the proteins polycystin-1 and -2, respectively [6]. Aberrant molecular mechanisms in the disease include proliferation and cell dedifferentiation, inflammation and complement activation, fibrosis and metabolic reprogramming toward a Warburg-like effect [7–9].

The vasopressin 2 receptor (V2R) antagonist tolvaptan is the first and only drug approved by the EMA and FDA for the treatment of ADPKD patients with rapid disease progression. Unfortunately, its use is limited by reduced tolerability due to aquaretic effects and risk for hepatotoxicity [10]. Therefore, the search for a more

effective drug that can reduce the progression of ADPKD continues. Potential drug candidates must have a strong safety and tolerability profile, as the disease requires lifelong treatment [11]. Due to the high costs and long timelines in drug development of new drug entities, drug repurposing has been considered in the search for new treatment options for ADPKD. This strategy utilizes existing compounds with known pharmacokinetic and safety profiles for new clinical indications [1].

Repurposing candidates have been tested for their cyst-reducing effects in vivo in various *Pkd1* knockout or conditional knockout mouse models [12]. Alternatively, mouse cells with a knockdown of *Pkd1* or post-nephrectomy renal epithelial cells derived from ADPKD patients [13, 14] can be cultured in a 3D format to better mimic the morphology of the in vivo state. In these models, cyst swelling can be induced by the addition of forskolin or desmopressin, and the compounds can then be screened for their capacity to inhibit cyst swelling.

Transcriptional gene profiling has been used to characterize mouse and human ADPKD kidneys [15–17], revealing alterations in a large number of genes associated with renal development, cell cycle progression, hypoxia, mitogen-mediated proliferation, epithelial–mesenchymal transition, aging, and immune/inflammatory responses [15]. However, mRNA and protein expression correlate poorly [18] and the vast majority of targets of approved drugs are proteins, not transcripts [19]. Since any in vitro model needs to be well characterized to ensure its relevance for the intended purpose, proteomic profiling of ADPKD in vitro models and tissues provides a more relevant characterization and validation of the model system. Furthermore, differentially expressed proteins (DEPs) may be of interest as new targets [1].

Here, we investigated the proteomes of healthy and late-stage ADPKD patient-derived 3DCC as well as donor-matched reference tissues using mass spectrometry-based global proteomics. We compared the ADPKD pathophysiology in the 3DCC with that in the matched tissues. We identified and quantified seven clinically relevant drug transporters, four drug-metabolizing enzymes, and 19 drug targets both in vitro and in vivo. Finally, we confirmed the function of the target proteins by investigating the cyst-reducing effects of drug repurposing candidates. In conclusion, our 3DCCs largely maintain the disease phenotype. Target proteins for previously identified promising drug repurposing candidates had comparable expression in vitro and in tissues. Exposure to drug repurposing candidates acting via the identified target proteins inhibited cyst swelling in vitro, supporting the suitability of the 3D in vitro model in screening of ADPKD repurposing candidates.

2 | Methods

All materials and suppliers are summarized in the [Supporting Information](#).

2.1 | Healthy and Diseased Renal Tissue

Healthy human reference kidney tissues (TH: tissue, healthy) were obtained from BioIVT (donor 2) and processed by Crown Bioscience Netherlands B.V. (donor 1). ADPKD patient tissue

at end-stage kidney disease ($n=3$; TD: tissue, diseased) was obtained after full nephrectomy. Tissue donors signed an informed consent according to the regulations of the Leiden University Medical Center (LUMC) (ref. NIER-23/SH/sh). The ADPKD patients had the following mutations: donor 3 (*PKD1* mutation: c.10594C>T p.Gln3532*), donor 4 (*PKD1* mutation: c.5622G>A p.Trp1874*), and donor 5 (*PKD2* mutation: c.1774C>T p.Arg592*). From each donor, small tissue samples were snap frozen in liquid nitrogen directly upon sampling and stored at -80°C until analysis as tissue samples. Three technical replicates, i.e., individual sample preparations from tissue homogenates, were analyzed from every biological replicate.

2.2 | Healthy and Diseased 3D Cyst Culture

Cells were isolated from the healthy (donor 1) and three diseased tissues (donor 3–5). 3DCC were established and maintained as described previously [13, 14]. Briefly, both the healthy (CH: cyst culture, healthy) and ADPKD patient (CD: cyst culture, diseased) cells were mixed with PrimCyst-Gel and then expanded in droplet culture in 6-well plates. After gel polymerization, PrimKidney medium was added. Cells were grown in the gel matrix for 6–8 days before splitting, for 3 weeks to create working stock cultures. Working stock cultures were then further expanded an additional 3 weeks to assay-ready cultures. At this time point, the cells were also used in the 3D cyst assay. Three technical replicates, i.e., individual sample preparations from individual 3D cyst cultures, were analyzed from every biological replicate.

2.3 | 3D Cyst Assay Using Primary Kidney Cells

Both healthy and patient-derived primary cyst assays were executed as previously described [13]. Briefly, cells were mixed with PrimCyst-Gel and plated in 384-well plates using a CyBio Felix 96/60 robotic liquid dispenser. The gel-cell mix was plated at a final cell density of 450 cell clusters per well. Cells were grown in the gel for 24 h, after which they were co-exposed to forskolin or ddAVP and test compounds. Optimal compound concentrations were selected from pilot dose–response experiments. After 48 h, cultures were fixed and processed as described in the [Supporting Information](#) for the 3D cyst assay using the *mIMCD3 Pkd1^{-/-}* cell line. Experiments were conducted in quadruplicate on two independent occasions.

2.4 | Quantitative Global Proteomic Analysis of Human Kidney Tissues and Cells

The cryopreserved 3DCCs and tissues were thawed and lysed, and the proteins were denatured at 95°C . Sample preparation for proteomic analysis followed a modified sp3 protocol [20], using endoproteinase LysC and trypsin. Peptides were separated on an EASY-spray C_{18} -column (50 cm, $75\ \mu\text{m}$ inner diameter), using an acetonitrile/water gradient (0.1% formic acid) at 300 nL/min and analyzed on an Orbitrap Q Exactive HF mass spectrometer. The raw MS data files were processed with MaxQuant [21] using the UniProtKB/Swiss-Prot reference

human proteome database [22]. Data analysis was performed in amica [23], Perseus [24] and using an in-house developed proteomics data pipeline in R (version 4.3.1). Differential expression analysis was performed with DEqMS [25] (p -value ≤ 0.05 ; min. absolute log2fold enrichment ≥ 1) in amica and gene set enrichment analysis (GSEA; p -value ≤ 0.05 ; multiple testing correction with Benjamini-Hochberg method) with clusterProfiler [26] (version 3.18) in R. Protein abundances (fmol/ μg total protein) were calculated with the Total Protein Approach [27]. To ensure high-quality quantification, only proteins identified with at least three unique + razor peptides were considered to be quantified. The mass spectrometry proteomics data have been deposited to the ProteomeXchange Consortium via the PRIDE [28] partner repository with the dataset identifier PXD056281. See [Supporting Information](#) for details.

2.5 | Statistical Analysis

Unless otherwise stated, statistical analysis and plot generation were carried out using GraphPad Prism version 9.0.0. Each sample was analyzed in three technical replicates, i.e., individual sample preparations, with three additional technical replicates, i.e., individual LC–MS/MS runs, yielding a total of nine proteomes per condition. Results are presented as mean values \pm SD of all biological and technical replicates. Technical replicates were strongly correlated throughout (average Pearson's r of 0.94–0.99; Figure S1).

3 | Results

3.1 | Global Proteomes of Healthy and Diseased Human Kidney

We identified 6718 proteins and quantified 5947 proteins across all samples by label-free quantitative global proteomic analysis of healthy and ADPKD 3DCCs and reference tissues (Figure 1a; Table S5). Of these, 4661 (85%) and 4268 (84%) proteins were shared across the 3DCCs and tissue samples, respectively (Figure 1b). Scatter plots and corresponding Spearman correlations (Figure 1c, Figure S2) and principal component analysis (PCA; Figure 1d) highlighted the differences between 3DCCs and tissue samples. As expected, the 3DCC samples showed a lower intragroup variance than the tissue samples due to their greater cellular homogeneity. The principal component loadings are presented in Figure S3 and Table S1.

The expression of tubular segment markers (Figure 1e, Table S1) was analyzed to characterize tubular cell types in 3DCC and tissue samples. Protein abundances were more comparable between healthy tissue (TH) and diseased tissue (TD) than between healthy cyst cultures (CH) and diseased cyst cultures (CD). CD showed a higher expression of proximal tubular and collecting duct markers and a lower expression of distal tubular markers compared to CH. Overall, the proximal tubular markers were approximately 100-fold and 20-fold more abundant than the distal tubular marker, SLC12A3, and the marker of the collecting duct, AQP2, respectively, which is consistent with the fact that proximal tubular cells make up the majority (more than 90%) of renal tubular cells [29].

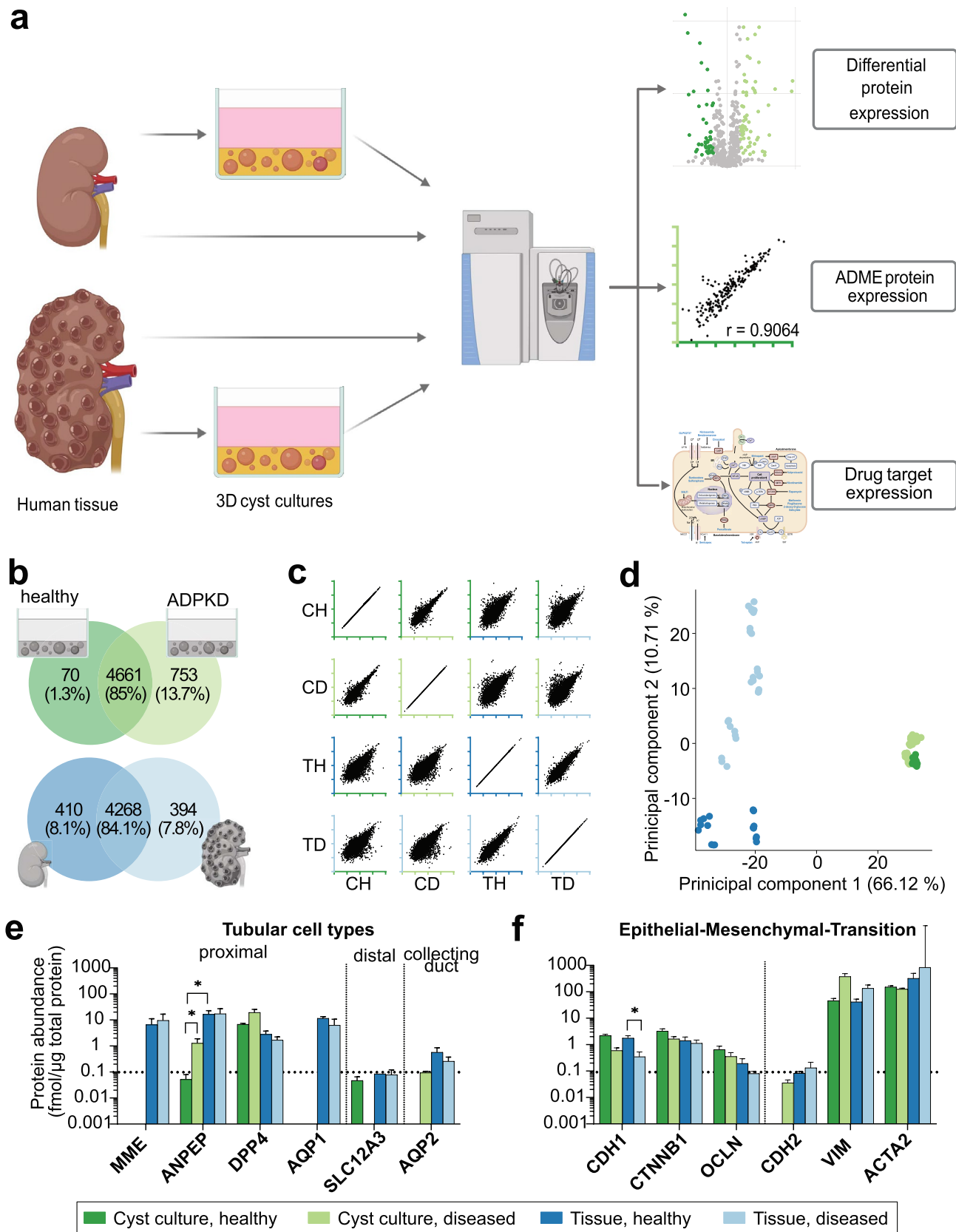


FIGURE 1 | Legend on next page.

FIGURE 1 | Global proteomic analysis of human healthy and ADPKD patient-derived 3DCCs and kidney tissues. (a) Outline of the present study. (b) Venn diagrams representing the overlap of quantified proteins in 3DCCs and tissues. (c) Correlations between protein levels across all sample types. (d) Principal component analysis (PCA) with each dot representing one sample replicate. Protein concentration plots of selected marker proteins for (e) tubular cell types and (f) epithelial–mesenchymal–transition with mean values \pm SD of all biological and technical replicates ($n_{\text{CH}} = 9$, $n_{\text{CD}} = 27$, $n_{\text{TH}} = 18$, $n_{\text{TD}} = 27$).

ADPKD is characterized by increased proliferation and partial dedifferentiation, i.e., epithelial-to-mesenchymal transition (EMT) [7]. In our samples, protein expression of the epithelial marker E-cadherin (CDH1) was significantly lower in TD than in TH (Figure 1f, Table S1). Although no other EMT markers showed significant differences, epithelial markers were generally more abundant in healthy samples, while mesenchymal or proliferative markers were more abundant in diseased samples. CDH1 and N-cadherin (CDH2) are also markers for distal and proximal tubular segments, respectively [30]. Thus, decreased CDH1 expression and increased CDH2 expression in CD compared to CH align with the observed tubular cell type proportions (Figure 1e).

Cell–cell junction proteins, crucial for barrier function, cell–cell communication, adhesion, and cell signaling, were more highly expressed in 3DCC samples than in tissues (Figure S4, Table S1). Expression of these proteins was generally decreased in diseased samples compared to healthy samples, though not statistically significant. In contrast, fibrotic (Figure S5, Table S1) and vascular markers (Figure S6, Table S1) were partially absent in 3DCCs in line with their greater cellular homogeneity. The expression of the majority of fibrotic markers was increased in diseased samples, with significant differences in Matrilysin (MMP7) and Tenascin (TNC). There was no clear trend in the expression of vascular markers, with only von Willebrand factor (VWF) significantly increased in TD compared to TH.

3.2 | Differential Expression Analysis of Healthy and Diseased 3DCCs

Differential expression analysis of proteins quantified in healthy and ADPKD 3DCC (Figure 2a) resulted in 104 DEPs (Figure 2b, Table S2), with 44 significantly downregulated and 60 significantly upregulated proteins in CD (adjusted p -values between 1.7×10^{-29} and 0.029). For a better understanding of the biological differences, gene set enrichment analysis was performed where the normalized enrichment score reflects the degree of gene set overrepresentation at the top or bottom of a ranked list of genes based on their logarithmic fold change. Here, gene set enrichment analysis (Figure 2c, Table S3) revealed that key pathways upregulated in CD include: biological oxidations, diseases of metabolism, and innate immune system including the nuclear factor NF-kappa-B (NF- κ B) pathway (DEPs in Figure 2d–f, Table S1). Downregulated pathways in CD included SLC transporter disorders, SUMOylation, and mRNA splicing (DEPs in Figure 2g–i). Inflammation and metabolic reprogramming previously described in ADPKD [7, 9] were also reflected in the 3D cyst proteomes (Figure 2e,f). In addition, reduced mRNA splicing (Figure 2i) and post-translational modification by

SUMOylation (Figure 2h) suggest reduced protein synthesis in the diseased cultures. Proteins of major proliferative signaling pathways involved in cyst growth [5, 7, 31] like JAK–STAT, PI3K/Akt, AMPK/mTOR, MAPK/ERK, Wnt/ β -catenin were quantified in both CH and CD but were not differentially expressed. Other pathophysiological changes in ADPKD [7, 32] such as fibrosis and changes in wound healing were not represented in the epithelial cell cultures, as they lack the fibroblasts and vessels involved in these processes.

3.3 | Differential Expression Analysis of Healthy and Diseased Patient Tissues

To generate reference data for comparison with the 3D cyst model, we analyzed differential protein expression between matched diseased and healthy tissues, identifying 186 DEPs (Figure 3a, Table S2)—74 downregulated and 112 upregulated in TD (adjusted p -values between 3.3×10^{-22} and 0.045). Consistent with inflammation (Figure 2f) and metabolic reprogramming (Figure 2e) observed in the 3D cyst model, gene set enrichment analysis (Figure 3b, Table S3) showed that the complement cascade (DEPs in Figure 3c, Table S1) was upregulated, while fatty acid metabolism (DEPs in Figure 3f), and the citric acid (TCA) cycle and respiratory electron transport (DEPs in Figure 3h) were downregulated in TD. Similarly, as observed in the 3DCCs (Figure 2h,i), TD samples displayed reduced mitochondrial translation, particularly mitochondrial tRNA aminoacylation (DEPs in Figure 3g), confirming mitochondrial dysfunction in the disease [9]. Consistent with previously described changes in wound healing and fibrosis in ADPKD [7, 32], platelet degranulation (DEPs in Figure 3d) and extracellular matrix organization and interactions (DEPs in Figure 3e) were among the upregulated pathways in TD that were not detectable in the 3DCCs, due to their greater cellular homogeneity.

Among the proteins involved in proliferative signaling pathways commonly upregulated in ADPKD, only STAT1 was upregulated in TD. Overall, despite the perceived heterogeneity of the tissue samples and the limited number of samples, our pathway analysis aligned with previous transcriptome findings [15, 16, 33] and highlighted alterations of protein synthesis pathways as a hallmark of ADPKD. Further, a good agreement between the DEPs in ADPKD 3DCCs and tissues supports the potential of 3DCCs as an in vitro model for ADPKD drug screening.

3.4 | ADME-Related Proteins in Healthy and Diseased Human Kidney

Since drug exposure to the target cells can be influenced by drug transporting and drug-metabolizing proteins, we analyzed the expression of these in the 3DCCs and tissues. Of the

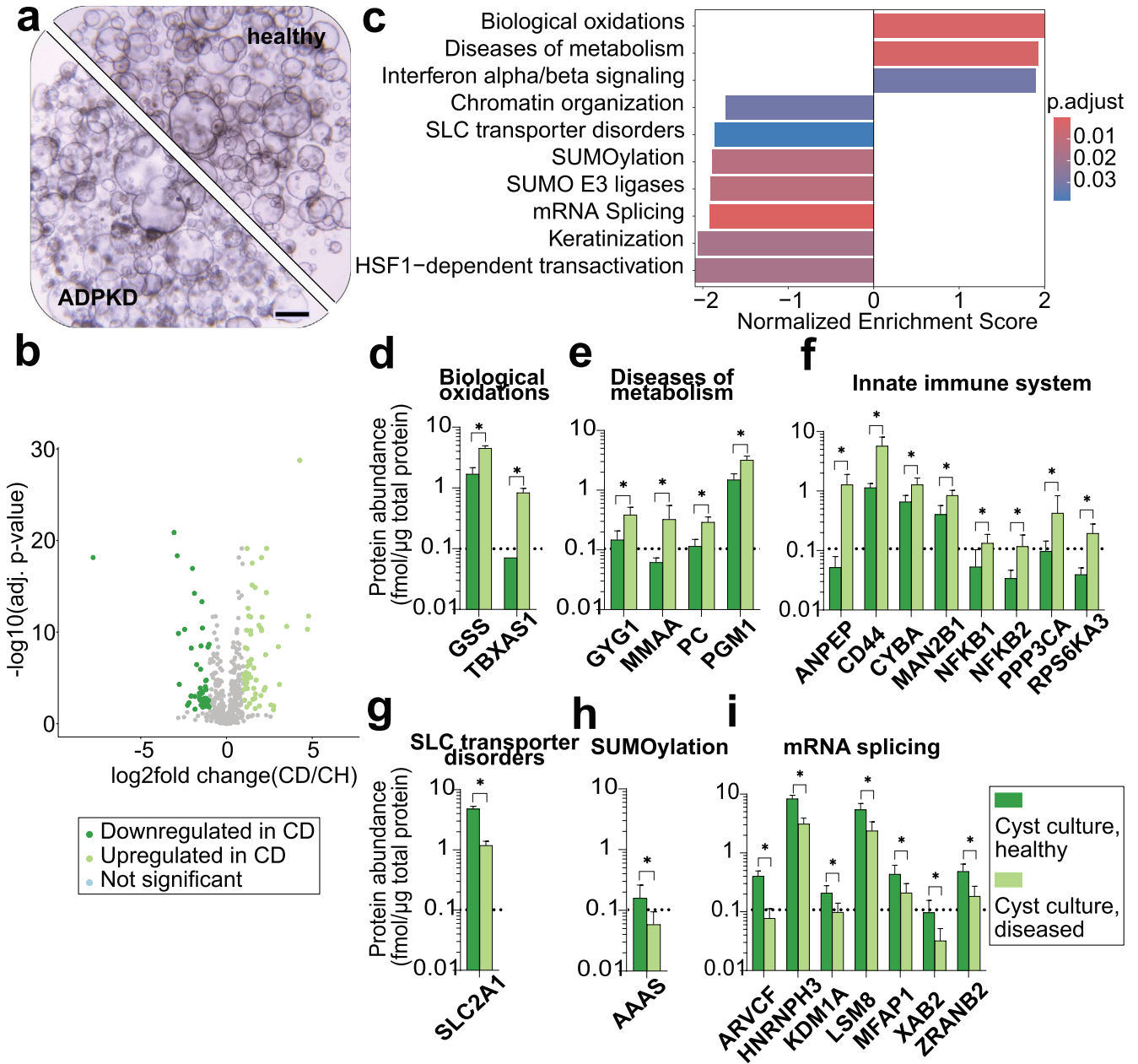


FIGURE 2 | Differential protein expression in healthy and diseased 3DCCs. (a) Representative light micrographs of healthy and ADPKD 3DCCs. Scale bar = 100 μm. (b) Volcano plot with significantly downregulated and upregulated proteins in the ADPKD 3DCCs. (c) Summary of gene set enrichment analysis with selected downregulated (left) and upregulated (right) Reactome pathways in ADPKD 3DCCs. The plot is sorted based on the normalized enrichment score. (d) Protein concentration plots of differentially expressed proteins related to biological oxidations; (e) diseases of metabolism; (f) innate immune system; (g) SLC transporter disorders; (h) SUMOylation; (i) mRNA splicing with mean values ± SD of all biological and technical replicates ($n_{CH} = 9$, $n_{CD} = 27$).

682 ADME-related proteins compiled by Schröder et al. [34], we quantified 290 across all samples, with 87% (217 proteins) and 88% (231 proteins) shared between 3DCCs and tissue samples, respectively (Figure 4a). The correlation of ADME protein abundances between healthy and diseased 3DCCs (Spearman correlation $r = 0.9064$; Figure 4b) and tissues ($r = 0.9355$; Figure 4b) was high. Most of the clinically important drug transporters [36] were detected at low abundances in tissues, with no significant differences between TH and TD (Figure 4c,d; Tables S1, S4). Some transporters recommended for evaluation during drug

development in previous guidelines [37], OCTN2 (*SLC22A5*), OAT4 (*SLC22A11*), and URAT1 (*SLC22A12*), were quantified, while other clinically relevant renal transporters OAT2 (*SLC22A7*), THTR2 (*SLC19A3*), and PEPT2 (*SLC15A2*) were below the limit of detection or, in the case of MATE1 (*SLC47A1*), MATE2-K (*SLC47A2*), and ENT1 (*SLC29A1*), were detected but not quantified according to our strict requirement for quantification (see methods). In vitro, the anion transport axis OAT/MRP was preserved, while the cation transport axis OCT/MATE was below detection limit.

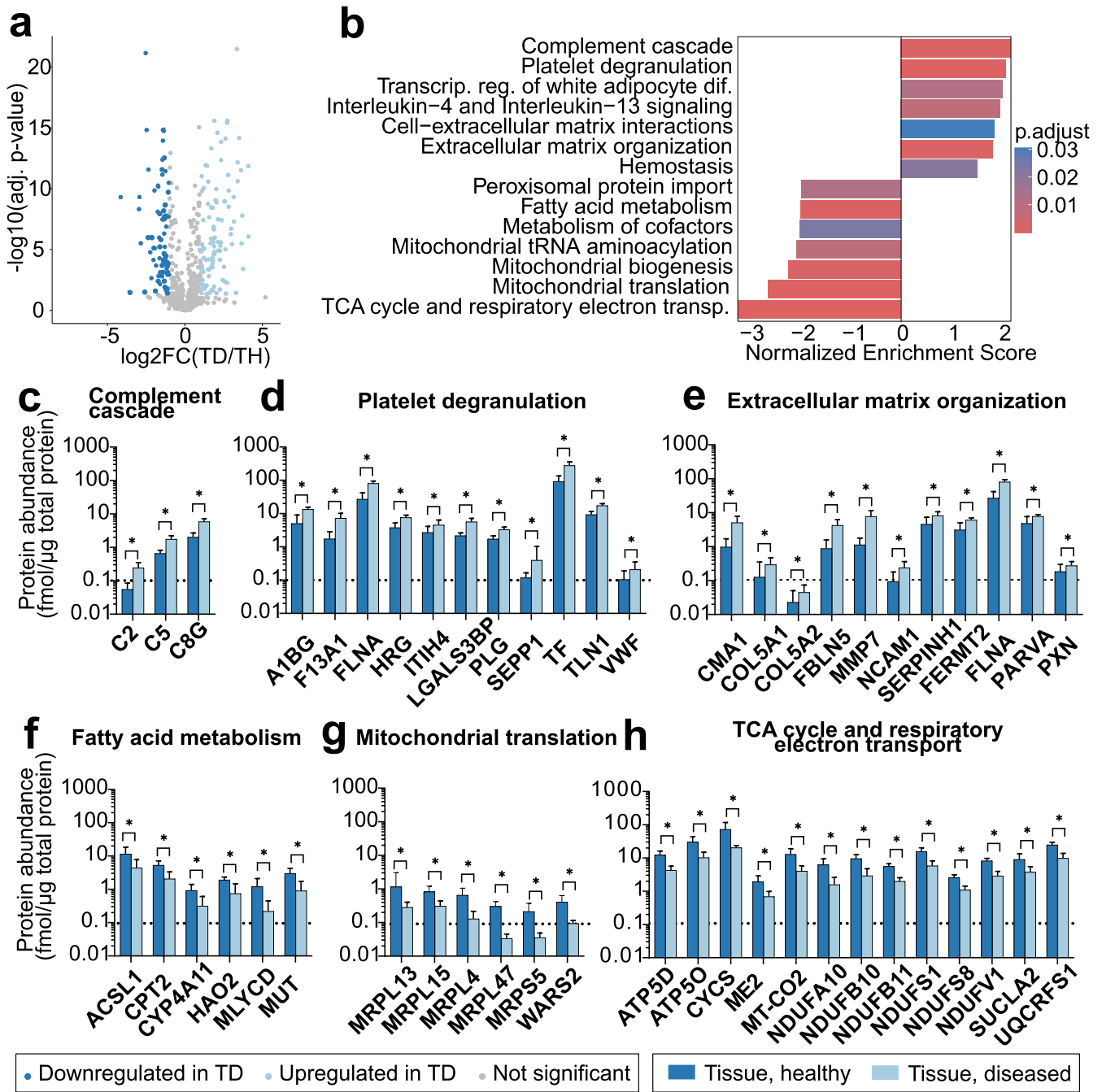


FIGURE 3 | Differential protein expression in healthy and diseased patient tissues. (a) Volcano plot with significantly downregulated and up-regulated proteins in the ADPKD tissues. (b) Summary of gene set enrichment analysis with selected downregulated (left) and upregulated (right) Reactome pathways in ADPKD tissues. The plot is sorted based on the normalized enrichment score. (c) Protein concentration plots of differentially expressed proteins related to complement cascade; (d) Platelet degranulation; (e) ECM organization and interactions; (f) fatty acid metabolism; (g) mitochondrial translation; (h) TCA cycle and respiratory electron transport with mean values \pm SD of all biological and technical replicates ($n_{TH} = 18$, $n_{TD} = 27$).

The renal drug-metabolizing enzymes CYP3A5 (*CYP3A5*), UGT1A6 (*UGT1A6*), UGT1A9 (*UGT1A9*), and UGT2B7 (*UGT2B7*) were quantified in at least one 3DCC or tissue sample (Figure 4d, Tables S1, S4) with UGT1A6 significantly higher in CH than CD. UGTs 1A9 and 2B7 [38] were only quantified in tissues. Overall, fewer drug transporters and drug-metabolizing enzymes were quantified in 3DCCs compared to tissues, consistent with previous observations in other renal tubular cell culture models [39, 40].

In addition to drug transporters, we analyzed the expression of renal tubular transporters of proteins, electrolytes, glucose, and urate (Figure S7, Table S1), essential for maintaining renal function. No significant differences in the expression of these transporters were found between healthy and diseased samples. As observed for drug transporters, expression levels of these transport proteins were barely maintained in vitro, as most transporters were below the detection limit. We can therefore not exclude

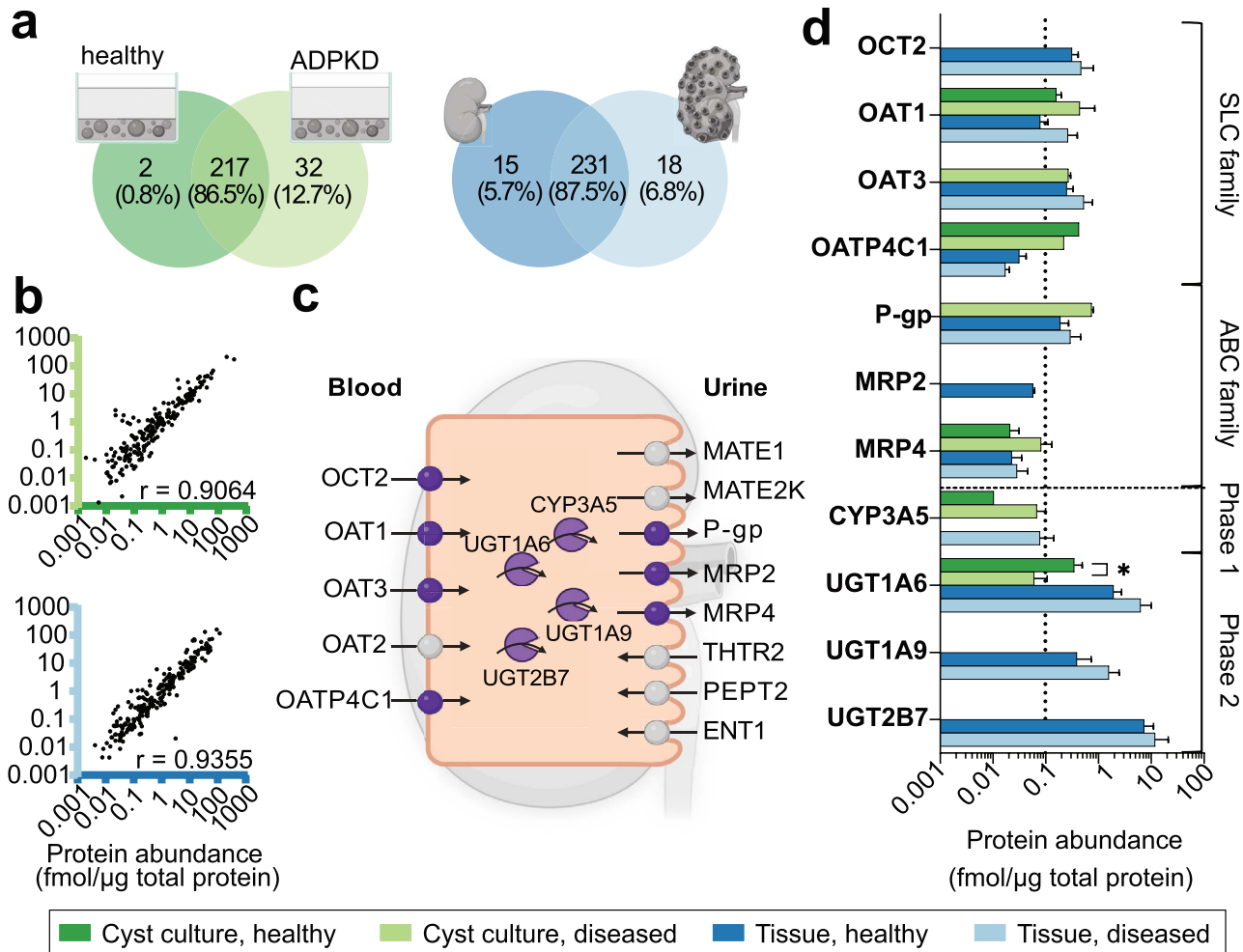


FIGURE 4 | ADME (absorption, distribution, metabolism, excretion) protein expression in human healthy and ADPKD patient-derived 3DCCs and kidney tissues. (a) Venn diagrams representing the overlap of quantified ADME proteins in 3DCCs and tissues. (b) Linear correlation plots of ADME protein expression in 3DCCs and tissues. (c) Clinically important transporters and enzymes in renal proximal tubular cells (modified from Galetin et al. [35]). Proteins highlighted in purple were quantified in our samples while proteins in gray were below the limit of detection. (d) Protein concentrations of clinically relevant drug transporters (SLC and ABC families) and phases 1 and 2 drug-metabolizing enzymes with mean values \pm SD of all biological and technical replicates ($n_{CH} = 9$, $n_{CD} = 27$, $n_{TH} = 18$, $n_{TD} = 27$).

that differences between diseased and healthy samples were below the resolution limit.

3.5 | ADPKD Repurposing Candidates Inhibit Cyst Swelling In Vitro

18 potential repurposing candidates for ADPKD and their respective targets were recently summarized by Zhou and Torres [1]. We investigated if these drug targets were present in the 3DCCs. For two of the drugs (probutol and elamipretide), molecular targets were not defined and they were therefore excluded. The remaining 16 drugs, along with their putative target proteins and/or key regulators in ADPKD, and their expression levels in 3DCCs and tissues are summarized in Figure 5a,b and Table 1. We also included the approved drug tolvaptan, the SMAC mimetic birinapant [2], and the mTOR inhibitor rapamycin. Of the 39 targets, we quantified 19 proteins—16 in

3DCCs and 16 in tissues (Figure 5a,b; Table S1). As previously observed, AVPR2, the target of tolvaptan, was below the limit of detection. Importantly, its expression in 3DCCs was confirmed by gene expression analysis (unpublished data). Previous phenotypic screens in murine ADPKD 3DCCs showed a reduction of cyst size through treatment with the repurposing candidates birinapant [2] and pioglitazone [3], although pioglitazone was not effective in mice. Here, we complemented these results with our own studies in mouse and human ADPKD 3DCCs to expand the number of involved targets (Figure 5c,d; Table 2). The AMPK activators metformin and pioglitazone, the glycolysis inhibitor 2-deoxy-D-glucose, the NRF2 activator bardoxolone, the SMAC mimetic birinapant, and the mTOR inhibitor rapamycin all inhibited cyst swelling in vitro. Additionally, another study recently demonstrated that the direct and specific allosteric AMPK activator PXL770 inhibits cyst swelling in human 3DCCs [13]. Lastly, in line with its mechanism of action, tolvaptan only inhibits cyst swelling when cyst growth is induced through

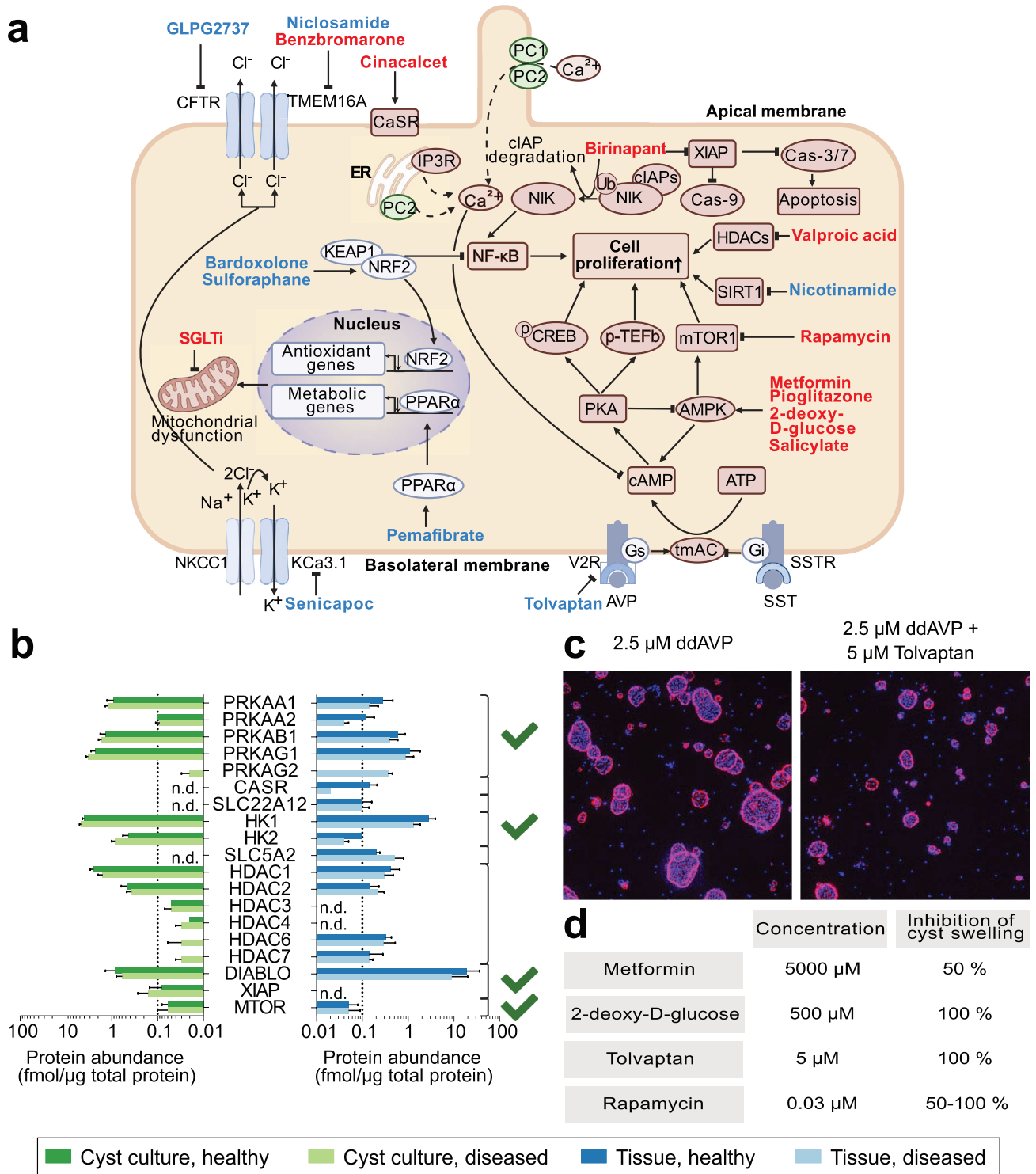


FIGURE 5 | Protein quantification of ADPKD drug targets. (a) Schematic illustration of the key mechanisms of ADPKD pathogenesis and dys-regulated signaling pathways targeted by potential repurposing candidates, modified from Zhou and Torres [1]. Drug targets, key regulators and the drug candidates targeting these that were detected in the ADPKD 3DCCs and tissues are highlighted in red. (b) Protein abundance of drug targets and/or key regulators in 3DCC and tissue samples with mean values \pm SD of all biological and technical replicates (n_{CH} = 9, n_{CD} = 27, n_{TH} = 18, n_{TD} = 27). Targets that upon drug engagement reduced cyst size in human and/or mouse ADPKD 3D cyst swelling assay are marked with green ticks [2–4]. (c) Representative image of the phenotypic ADPKD 3D cyst assay with swelling inducer desmopressin (ddAVP) alone (left) and together with tolvaptan (right). Cytoskeleton in red and nuclei in blue. (d) Functional response of human ADPKD 3DCCs to exposure with ADPKD repurposing candidates and cyst swelling inducer desmopressin (ddAVP).

TABLE 1 | Protein expression of target proteins of drug candidates.

Drug candidates	Targets ^b	Gene names	Tissue, healthy ^a			Tissue, diseased ^a			Cyst culture, healthy ^a			Cyst culture, diseased ^a					
			Mean	SD	N	Mean	SD	N	Mean	SD	N	Mean	SD	N	Significance		
Metformin ^c , Salsalate	AMPK	PRKAA1	0.28	0.18	14	0.14	0.08	22	ns	0.90	0.37	9	1.23	0.15	27	ns	
			PRKAA2	0.12	0.06	14	0.04	0.01	4	ns	0.10	NA	1	0.09	0.02	12	ns
			PRKAB1	0.60	0.26	16	0.39	0.20	12	ns	1.34	0.45	9	1.66	0.29	27	ns
		PRKAB2	NA	NA	0	NA	NA	0	ns	NA	NA	0	NA	NA	0	ns	
		PRKAG1	1.09	0.73	18	0.88	0.43	26	ns	2.27	0.56	9	3.26	0.39	27	ns	
		PRKAG2	NA	NA	0	0.36	0.09	2	ns	NA	NA	0	0.02	0.01	4	ns	
Oxypurinol	Xanthine oxidase (endothelial dysfunction, crystalluria)	PRKAG3	NA	NA	0	NA	NA	0	ns	NA	NA	0	NA	NA	0	ns	
		XDH	NA	NA	0	NA	NA	0	ns	NA	NA	0	NA	NA	0	ns	
Cinacalcet	CaSR, cAMP	CASR	0.14	0.07	13	0.02	NA	1	ns	NA	NA	0	NA	NA	0	ns	
GLPG2737 ^c	CFTR	CFTR	NA	NA	0	NA	NA	0	ns	NA	NA	0	NA	NA	0	ns	
Benzbromarone	TMEM16A (see below), URAT	SLC22A12	0.10	0.06	14	0.10	0.04	9	ns	NA	NA	0	NA	NA	0	ns	
Niclosamide	TMEM16A (many other targets)	ANO1	NA	NA	0	NA	NA	0	ns	NA	NA	0	NA	NA	0	ns	
Senicapoc	KCa3.1	KCNN4	NA	NA	0	NA	NA	0	ns	NA	NA	0	NA	NA	0	ns	
Pioglitazone ^c	PPARγ, AMPK (see above)	PPARG	NA	NA	0	NA	NA	0	ns	NA	NA	0	NA	NA	0	ns	
2-deoxy-D-glucose	Glycolysis	HK1	2.75	1.17	18	1.28	0.54	27	ns	3.96	0.39	9	4.62	0.43	27	ns	
		HK2	0.10	NA	1	0.04	0.01	2	ns	0.43	0.14	9	0.85	0.16	27	ns	
		HK3	NA	NA	0	NA	NA	0	ns	NA	NA	0	NA	NA	0	ns	
SGLT2 inhibitor ^c	Tubulo-glomerular feedback, metabolism	GCK	NA	NA	0	NA	NA	0	ns	NA	NA	0	NA	NA	0	ns	
		SLC5A2	0.20	0.04	6	0.51	0.28	16	ns	NA	NA	0	NA	NA	0	ns	

(Continues)

TABLE 1 | (Continued)

Drug candidates	Targets ^b	Gene names	Tissue, healthy ^a			Tissue, diseased ^a			Cyst culture, healthy ^a			Cyst culture, diseased ^a			
			Mean	SD	N	Mean	SD	N	Mean	SD	N	Mean	SD	N	Significance
Pemafibrate	PPAR α		NA	NA	0	NA	NA	0	NA	NA	0	NA	NA	0	ns
Bardoxolone ^c , Sulforaphane	NRF2		NA	NA	0	NA	NA	0	NA	NA	0	NA	NA	0	ns
Valproic acid	HDAC		0.41	0.25	16	0.30	0.17	26	2.49	0.45	9	1.58	0.40	27	ns
			0.15	0.08	9	0.22	0.08	7	0.47	0.15	8	0.37	0.10	27	ns
			NA	NA	0	NA	NA	0	0.05	0.00	5	0.05	0.02	19	ns
			NA	NA	0	NA	NA	0	0.02	0.00	8	0.03	0.01	27	ns
			NA	NA	0	NA	NA	0	NA	NA	0	NA	NA	0	ns
			0.32	0.11	18	0.29	0.23	16	0.01	0.00	2	0.03	0.03	24	ns
			0.14	0.14	9	0.14	0.03	8	NA	NA	0	0.03	0.01	7	ns
			NA	NA	0	NA	NA	0	NA	NA	0	NA	NA	0	ns
			NA	NA	0	NA	NA	0	NA	NA	0	NA	NA	0	ns
			NA	NA	0	NA	NA	0	NA	NA	0	NA	NA	0	ns
			NA	NA	0	NA	NA	0	NA	NA	0	NA	NA	0	ns
Nicotinamide ^c	Sirtuin		NA	NA	0	NA	NA	0	NA	NA	0	NA	NA	0	ns
Tolvaptan	Vasopressin receptor 2		NA	NA	0	NA	NA	0	NA	NA	0	NA	NA	0	ns
Birinapant	SMAC		18.54	17.29	17	8.94	10.97	17	0.86	0.51	8	0.59	0.21	25	ns
			NA	NA	0	NA	NA	0	0.08	0.07	8	0.16	0.11	26	ns
			NA	NA	0	NA	NA	0	NA	NA	0	NA	NA	0	ns
			NA	NA	0	NA	NA	0	NA	NA	0	NA	NA	0	ns
Rapamycin	mTOR		0.05	0.03	13	0.05	0.04	13	0.06	0.02	9	0.06	0.04	27	ns

^aConcentrations are given in fmol/ μ g total protein.^bTargets discussed for ADPKD treatment. Some of the drugs have targets that are not considered for ADPKD treatment and are not listed here.^cAlready ongoing clinical trial for ADPKD.

TABLE 2 | Functional response of human and mouse ADPKD 3D cyst cultures to exposure with ADPKD repurposing candidates and cyst swelling inducer forskolin (FSK).

Drug	Concentration	Assay tested	Inhibition of swelling
Metformin	5000 μ M	mouse	50% inhibition
Metformin	5000 μ M	human	50% inhibition
Pioglitazone [3]	10 μ M	mouse	100% inhibition, slight cytotoxicity
2-deoxy-D-glucose	5000 μ M	human	50%–100% inhibition
Bardoxolone Methyl	10 μ M	mouse	100% inhibition, cytotoxic
Tolvaptan	5 μ M	mouse	No effect
Tolvaptan	5 μ M	human	No effect
Birinapant [2]	100 μ M	mouse	100% inhibition
Rapamycin [2, 4]	0.03 μ M	mouse	50%–100% inhibition
Rapamycin	0.03 μ M	human	50%–100% inhibition

the vasopressin analogue desmopressin (ddAVP; see methods). We conclude that many proposed drug targets for treatment of ADPKD, including those affecting cell proliferation, can be investigated in 3DCCs.

4 | Discussion

In this study, we analyzed the proteomic signature and function of late-stage ADPKD patient-derived 3D cyst models for drug repurposing and donor-matched tissue references, resulting in three major findings.

First, our results indicate that the ADPKD 3DCCs largely mimic the cellular disease profile present in tissues. Maintaining a disease phenotype *in vitro* is challenging, and cell cultures can differ significantly from their parent tissues [41]. Importantly, the three ADPKD tissues and 3DCCs in our study were derived from the same patients, enabling reliable analysis of how well the 3DCCs represent the ADPKD kidney proteome. Despite the small sample size and probable differences in the sampling site of the small tissue piece and the combination of various tissue pieces for establishment of the cyst cultures, our results are remarkably consistent with previous studies based on human kidney transcriptomes [15, 16, 33], emphasizing the validity of this study.

Disease-relevant proliferation, metabolic reprogramming, and inflammatory responses [7, 9] were preserved in the 3DCCs. Similarly, gene set enrichment analysis of ADPKD tissues closely mirrored these processes, along with increased extracellular matrix disposition and hemostasis, reflecting the progressive fibrosis and altered wound healing [7, 32] associated with the disease. Additionally, downregulation of protein synthesis processes, namely mRNA splicing (transcription), mitochondrial translation, and SUMOylation (post-translational modification), was observed in both 3DCCs and ADPKD tissues, suggesting an overall reduced mitochondrial mass, which is in agreement with observations in mouse and rat models of ADPKD [42]. This is, however, in contrast to the hypothesis that

metabolic reprogramming occurs in ADPKD to ensure a net increase in biomass, including proteins, required for proliferation [9]. Activation of mTOR and stress kinases (eIF2K) and reduced activity of the protein synthesis inhibitor PERK (PKR-like ER kinase) suggest an increase in protein synthesis in proliferating ADPKD tissue [43]. Thus, whether protein synthesis is increased or decreased in ADPKD remains unclear.

Notably, no differential expression was observed for proteins involved in the proliferative signaling pathways PI3K/Akt, AMPK/mTOR, MAPK/ERK, and Wnt/ β -catenin. Most signaling pathways are mediated by phosphorylation and dephosphorylation cascades, suggesting that phosphoproteomics, rather than global proteomics, would be more appropriate for studying disease-associated changes in these pathways. While this analysis was beyond the scope of this study, ongoing work within the DRUGtrain consortium suggests differential phosphorylation of signaling pathways such as MAPK, mTOR, and PPAR in ADPKD tissues. Furthermore, our phenotypic 3DCC model captured cyst swelling inhibition through phosphorylation state dependent AMPK activation and mTOR inhibition following exposure to repurposing candidates.

Several proteomic studies of urinary exosomes from ADPKD patients have identified potential urinary biomarkers and target proteins for the treatment of ADPKD, including complement-related proteins [8], the PC1/TMEM2 or PC2/TMEM2 ratio [44], and proteins involved in cell proliferation and matrix remodeling [45], including the recent Matrix Metalloproteinase-7 [46]. Interestingly, differential expression of several of these biomarkers was confirmed in our tissue proteomes.

We observed large differences in the abundance of tubular cell types, with notably higher expression of proximal tubular epithelial marker proteins, which explains why few distal tubular and collecting duct markers were above the limit of detection in this bulk proteomics analysis. The dominance of the proximal tubular cells provides an explanation for the good agreement with the 3DCCs, which are also mainly composed of these cells. That said, there are at least 16 highly specialized renal epithelial

cell types accompanied by specialized endothelial cells, immune cells, and interstitial cell types, making renal tissue quite heterogeneous [47]. ADPKD kidneys additionally exhibit cystic and fibrotic regions and altered vascular architecture, further increasing the potential sample heterogeneity [48]. Indeed, we observed a trend toward higher expression of fibrotic markers in diseased samples compared to healthy samples (Figure S5). Consistent with the greater cellular homogeneity of 3DCCs, fibrosis and vascular marker proteins were more frequently and abundantly found in tissue samples. Overall, this indicates that the 3DCC model is not suitable for studies of ADPKD-induced interstitial fibrosis and vascular alterations.

Our second major finding is that relevant targets for drug repurposing are expressed in the 3DCCs. To complement our differential expression analysis for identification of putative drug targets, we analyzed the protein expression of targets of proposed drug candidates with proven efficacy in preclinical ADPKD models and FDA approval or phase 2/3 clinical trials for other diseases [1]. Thirteen (81%) of the 16 ADPKD targets identified in our kidney tissues were also found in the 3DCC. These targets participate in four different pathways investigated for drug interventions in ADPKD, which underscores the versatility of the 3DCC for screening of ADPKD drug candidates.

Increased cAMP levels in cystic tissues are central in ADPKD pathophysiology as they stimulate cell proliferation, and several strategies are targeting cAMP signaling to ameliorate cyst growth [35]. In turn, cAMP has been suggested to regulate AMPK activity [49] and several targets along this pathway can reduce cell proliferation in ADPKD, namely inhibition of glycolysis, activation of AMPK, and inhibition of mTOR. Targets for the glycolysis inhibitor 2-deoxy-D-glucose, AMPK activator metformin, and mTOR inhibitor rapamycin were quantified in both tissues and 3DCCs, suggesting that this central signaling pathway with proven in vivo efficacy [50] can be studied in our phenotypic 3DCC model.

Indeed, our third major finding shows that the 3D cyst model responds to repurposing candidates acting via these identified target proteins. In line with the quantification of target proteins in the human 3DCCs, up to 50% inhibition of cyst swelling through the AMPK activator metformin, and up to 100% inhibition through the glycolysis inhibitor 2-deoxy-D-glucose and the mTOR inhibitor rapamycin was observed in the phenotypic drug screening. While the expression of the V2R, the target of tolvaptan, was below the limit of detection, in vitro inhibition of cyst swelling by tolvaptan was still observed in the 3DCCs, only after stimulation with the receptor agonist ddAVP. Even though this indicates some discrepancy between quantified protein expression and functional response, the efficacy of tolvaptan in our assay suggests that drugs with target expression below the limit of detection might still inhibit cyst swelling in the 3DCCs. Conversely, all tested drugs with quantified targets showed in vitro efficacy. Importantly, most of the quantified target proteins are located intracellularly while fewer membrane-bound proteins were detected in our whole-cell homogenates. For the latter, membrane enrichment is suggested to elevate the abundance of these proteins beyond the limit of quantification and help identify less abundant drug target proteins, transporters, and drug-metabolizing enzymes [51].

The inversion of apicobasal polarity in renal tubular epithelial cells promotes cell proliferation and cyst enlargement in ADPKD [52], making it a key characteristic of the disease. While our proteomic analysis of bulk samples does not allow insights into cell polarity, we were able to quantify, among others, the polarity markers Na⁺/K⁺-ATPase and tight junction proteins 1–3. Immunofluorescent staining confirmed that the 3DCCs exhibit normal cell polarization with cilia protruding into the lumen (data not shown). The outward-facing basolateral membrane, which is in direct contact with the vasculature in vivo, can thus be exposed to potential drug candidates in vitro without concerns regarding partial inversion of the apicobasal polarity. Meanwhile, drug transporters expressed on the inward-facing apical membrane, often below the detection limit in our analysis, will therefore not affect the initial exposure of the cells to the repurposing candidates.

As samples from early-stage ADPKD patients were not included in our analysis, the results cannot be generalized to the entire ADPKD population. However, the 3DCCs and matching diseased tissues from end-stage renal disease patients analyzed here likely show the greatest contrast to healthy reference samples. They therefore reflect most of the disease-relevant changes that may remain unresolved in earlier stages of the disease. This presumption is supported by our findings throughout the study, where 3DCCs from late-stage ADPKD patients not only reflected significant disease-relevant changes in protein expression but also responded effectively to treatment with promising repurposing candidates.

In summary, our study comprehensively evaluates patient-derived 3DCCs and confirms the ADPKD pathophysiology of these cultures at the proteomic level. Quantified expression of drug target proteins provides a valuable resource for future drug repurposing efforts and target parameterization in ADPKD pharmacodynamic models. Finally, our phenotypic 3DCC assay effectively responds to key repurposing candidates and drugs such as AMPK activators, an mTOR inhibitor, and tolvaptan, indicating its versatility as an in vitro model for drug screening in ADPKD research.

Author Contributions

A.M. and P.A. wrote the manuscript. A.M. and P.A. designed the research. A.M., B.K., and M.I. performed the research. A.M. and B.K. analyzed the data. H.B., L.S.P., N.D., G.J.P.W., H.V., and D.J.M.P. contributed new reagents/analytical tools.

Acknowledgments

The authors would like to thank Imke Smits and Shannon Kouters at Crown Bioscience Netherlands B.V. for the generation of the primary tissue samples and performance of the phenotypic drug screens in the 3D cyst cultures. This project has received funding from the European Union's Horizon 2020 research and innovation programme under the Marie Skłodowska Curie grant agreement No 955879 (DRUGtrain). This work was supported by the Swedish Research Council grant (number 1951) for Per Artursson.

During the preparation of this work, the author(s) used ChatGPT to improve readability and language. The authors reviewed and edited the content as needed and take full responsibility for the content of the publication.

Figure 1a (BioRender.com/h60u937), Figure 1b (BioRender.com/k71r134), Figure 4a (BioRender.com/k71r134), Figure 4c (BioRender.com/z13h256), Figure 5a,b (BioRender.com/m92t047) created in BioRender. Meyer, A. (2024).

Conflicts of Interest

Authors M.I., H.B., and L.S.P. were employed by Crown Bioscience Netherlands B.V. Authors B.K., N.D., and H.V. were employed by J&J Innovative Medicine. All other authors declared no conflicts of interest.

References

1. J. X. Zhou and V. E. Torres, "Drug Repurposing in Autosomal Dominant Polycystic Kidney Disease," *Kidney International* 103 (2023): 859–871.
2. T. B. Malas, W. N. Leonhard, H. Bange, et al., "Prioritization of Novel ADPKD Drug Candidates From Disease-Stage Specific Gene Expression Profiles," *eBioMedicine* 51 (2020): 102585.
3. A. A. Kanhai, H. Bange, L. Verburg, et al., "Renal Cyst Growth Is Attenuated by a Combination Treatment of Tolvaptan and Pioglitazone, While Pioglitazone Treatment Alone Is Not Effective," *Scientific Reports* 10, no. 1 (2020): 1–12, <https://doi.org/10.1038/s41598-020-58382-z>.
4. T. H. Booij, H. Bange, W. N. Leonhard, et al., "High-Throughput Phenotypic Screening of Kinase Inhibitors to Identify Drug Targets for Polycystic Kidney Disease," *SLAS Discovery: Advancing Life Sciences R&D* 22 (2017): 974–984.
5. E. Cornec-Le Gall, A. Alam, and R. D. Perrone, "Autosomal Dominant Polycystic Kidney Disease," *Lancet* 393 (2019): 919–935.
6. E. Cornec-Le Gall, V. E. Torres, and P. C. Harris, "Genetic Complexity of Autosomal Dominant Polycystic Kidney and Liver Diseases," *Journal of the American Society of Nephrology* 29 (2018): 13–23.
7. C. Formica and D. J. M. Peters, "Molecular Pathways Involved in Injury-Repair and ADPKD Progression," *Cellular Signalling* 72 (2020): 109648.
8. M. Salih, J. A. Demmers, K. Bezstarosti, et al., "Proteomics of Urinary Vesicles Links Plakins and Complement to Polycystic Kidney Disease," *Journal of the American Society of Nephrology* 27 (2016): 3079–3092.
9. C. Podrini, L. Cassina, and A. Boletta, "Metabolic Reprogramming and the Role of Mitochondria in Polycystic Kidney Disease," *Cellular Signalling* 67 (2020): 109495.
10. V. E. Torres, A. B. Chapman, O. Devuyst, et al., "Tolvaptan in Patients With Autosomal Dominant Polycystic Kidney Disease," *New England Journal of Medicine* 367 (2012): 2407–2418.
11. A. A. Kiseleva and E. A. Golemis, "Informatics-Guided Drug Repurposing for Autosomal Dominant Polycystic Kidney Disease (ADPKD)," *eBioMedicine* 52 (2020): 102628.
12. C. J. Sieben and P. C. Harris, "Experimental Models of Polycystic Kidney Disease: Applications and Therapeutic Testing," *Kidney360* 4 (2023): 1155–1173.
13. P. G. Dagorn, B. Buchholz, A. Kraus, et al., "A Novel Direct Adenosine Monophosphate Kinase Activator Ameliorates Disease Progression in Preclinical Models of Autosomal Dominant Polycystic Kidney Disease," *Kidney International* 103 (2023): 917–929.
14. P. W. Brownjohn, A. Zoufir, D. J. O'Donovan, et al., "Computational Drug Discovery Approaches Identify Mebendazole as a Candidate Treatment for Autosomal Dominant Polycystic Kidney Disease," *Frontiers in Pharmacology* 15 (2024): 1397864.
15. X. Song, V. di Giovanni, N. He, et al., "Systems Biology of Autosomal Dominant Polycystic Kidney Disease (ADPKD): Computational Identification of Gene Expression Pathways and Integrated Regulatory Networks," *Human Molecular Genetics* 18 (2009): 2328–2343.
16. Y. Muto, E. E. Dixon, Y. Yoshimura, et al., "Defining Cellular Complexity in Human Autosomal Dominant Polycystic Kidney Disease by Multimodal Single Cell Analysis," *Nature Communications* 13 (2022): 6497.
17. L. F. Menezes, F. Zhou, A. D. Patterson, et al., "Network Analysis of a Pkd1-Mouse Model of Autosomal Dominant Polycystic Kidney Disease Identifies HNF4 α as a Disease Modifier," *PLoS Genetics* 8 (2012): e1003053.
18. C. Wegler, M. Ölander, J. R. Wiśniewski, et al., "Global Variability Analysis of mRNA and Protein Concentrations Across and Within Human Tissues," *NAR Genomics and Bioinformatics* 2, no. 1 (2019): lqz010, <https://doi.org/10.1093/nargab/lqz010>.
19. A. L. Hopkins and C. R. Groom, "The Druggable Genome," *Nature Reviews. Drug Discovery* 1 (2002): 727–730.
20. C. S. Hughes, S. Moggridge, T. Müller, P. H. Sorensen, G. B. Morin, and J. Krijgsveld, "Single-Pot, Solid-Phase-Enhanced Sample Preparation for Proteomics Experiments," *Nature Protocols* 14 (2019): 68–85.
21. S. Tyanova, T. Temu, and J. Cox, "The MaxQuant Computational Platform for Mass Spectrometry-Based Shotgun Proteomics," *Nature Protocols* 11 (2016): 2301–2319.
22. The UniProt Consortium, "UniProt: The Universal Protein Knowledgebase in 2023," *Nucleic Acids Research* 51, no. D1 (2023): D523–D531, <https://doi.org/10.1093/nar/gkac1052>.
23. S. Didusch, M. Madern, M. Hartl, and M. Baccarini, "Amica: An Interactive and User-Friendly Web-Platform for the Analysis of Proteomics Data," *BMC Genomics* 23 (2022): 817.
24. S. Tyanova, T. Temu, P. Sinitcyn, et al., "The Perseus Computational Platform for Comprehensive Analysis of (Prote)omics Data," *Nature Methods* 13 (2016): 731–740.
25. Y. Zhu, L. M. Orre, Y. Zhou Tran, et al., "DEqMS: A Method for Accurate Variance Estimation in Differential Protein Expression Analysis," *Molecular & Cellular Proteomics* 19 (2020): 1047–1057.
26. T. Wu, E. Hu, S. Xu, et al., "clusterProfiler 4.0: A Universal Enrichment Tool for Interpreting Omics Data," *Innovation* 2 (2021): 100141.
27. J. R. Wiśniewski and D. Rakus, "Multi-Enzyme Digestion FASP and the 'Total Protein Approach'-Based Absolute Quantification of the *Escherichia coli* Proteome," *Journal of Proteomics* 109 (2014): 322–331.
28. J. A. Vizcaino, A. Csordas, N. del-Toro, et al., "2016 Update of the PRIDE Database and Its Related Tools," *Nucleic Acids Research* 44 (2016): D447–D456.
29. J. Liao, Z. Yu, Y. Chen, et al., "Single-Cell RNA Sequencing of Human Kidney," *Scientific Data* 7 (2020): 4.
30. K. Hiratsuka, T. Monkawa, T. Akiyama, et al., "Induction of Human Pluripotent Stem Cells Into Kidney Tissues by Synthetic mRNAs Encoding Transcription Factors," *Scientific Reports* 9 (2019): 913.
31. J. P. Margaria, C. C. Campa, M. C. De Santis, E. Hirsch, and I. Franco, "The PI3K/Akt/mTOR Pathway in Polycystic Kidney Disease: A Complex Interaction With Polycystins and Primary Cilium," *Cellular Signalling* 66 (2020): 109468.
32. T. B. Malas, C. Formica, W. N. Leonhard, et al., "Meta-Analysis of Polycystic Kidney Disease Expression Profiles Defines Strong Involvement of Injury Repair Processes," *American Journal of Physiology. Renal Physiology* 312 (2017): F806–F817.
33. S. Friedrich, H. Müller, C. Riesterer, et al., "Identification of Pathological Transcription in Autosomal Dominant Polycystic Kidney Disease Epithelia," *Scientific Reports* 11 (2021): 15139.
34. A. Schröder, K. Klein, S. Winter, et al., "Genomics of ADME Gene Expression: Mapping Expression Quantitative Trait Loci Relevant for Absorption, Distribution, Metabolism and Excretion of Drugs in Human Liver," *Pharmacogenomics Journal* 13 (2013): 12–20.

35. V. E. Torres and P. C. Harris, "Strategies Targeting cAMP Signaling in the Treatment of Polycystic Kidney Disease," *JASN* 25 (2014): 18–32.
36. A. Galetin, K. L. R. Brouwer, D. Tweedie, et al., "Membrane Transporters in Drug Development and as Determinants of Precision Medicine," *Nature Reviews. Drug Discovery* 23, no. 4 (2024): 1–26, <https://doi.org/10.1038/s41573-023-00877-1>.
37. M. J. Zamek-Gliszczynski, V. Sangha, H. Shen, et al., "Transporters in Drug Development: International Transporter Consortium Update on Emerging Transporters of Clinical Importance," *Clinical Pharmacology & Therapeutics* 112 (2022): 485–500.
38. K. M. Knights, A. Rowland, and J. O. Miners, "Renal Drug Metabolism in Humans: The Potential for Drug–Endobiotic Interactions Involving Cytochrome P450 (CYP) and UDP-Glucuronosyltransferase (UGT)," *British Journal of Clinical Pharmacology* 76, no. 4 (2013): 587–602, <https://doi.org/10.1111/bcp.12086>.
39. S. E. Jenkinson, G. W. Chung, E. van Loon, N. S. Bakar, A. M. Dalzell, and C. D. A. Brown, "The Limitations of Renal Epithelial Cell Line HK-2 as a Model of Drug Transporter Expression and Function in the Proximal Tubule," *Pflügers Archiv / European Journal of Physiology* 464 (2012): 601–611.
40. P. F. Secker, L. Luks, N. Schlichenmaier, and D. R. Dietrich, "RPTEC/TERT1 Cells Form Highly Differentiated Tubules When Cultured in a 3D Matrix," *ALTEX* 35 (2018): 223–234.
41. C. Pan, C. Kumar, S. Bohl, U. Klingmueller, and M. Mann, "Comparative Proteomic Phenotyping of Cell Lines and Primary Cells to Assess Preservation of Cell Type-Specific Functions," *Molecular & Cellular Proteomics* 8 (2009): 443–450.
42. Y. Ishimoto, R. Inagi, D. Yoshihara, et al., "Mitochondrial Abnormality Facilitates Cyst Formation in Autosomal Dominant Polycystic Kidney Disease," *Molecular and Cellular Biology* 37, no. 24 (2017): e00337-17, <https://doi.org/10.1128/MCB.00337-17>.
43. V. Schaeffer and C. K. Abrass, "Mechanisms and Control of Protein Translation in the Kidney," *American Journal of Nephrology* 31 (2009): 189–201.
44. M. C. Hogan, J. L. Bakeberg, V. G. Gainullin, et al., "Identification of Biomarkers for PKD1 Using Urinary Exosomes," *Journal of the American Society of Nephrology* 26 (2015): 1661–1670.
45. M. Bruschi, S. Granata, L. Santucci, et al., "Proteomic Analysis of Urinary Microvesicles and Exosomes in Medullary Sponge Kidney Disease and Autosomal Dominant Polycystic Kidney Disease," *Clinical Journal of the American Society of Nephrology* 14 (2019): 834–843.
46. M. H. v. Heugten, C. J. Blijdorp, S. Arjune, et al., "Matrix Metalloproteinase-7 in Urinary Extracellular Vesicles Identifies Rapid Disease Progression in Autosomal Dominant Polycystic Kidney Disease," *Journal of the American Society of Nephrology* 35 (2023): 321–334, <https://doi.org/10.1681/ASN.0000000000000277>.
47. M. S. Balzer, T. Rohacs, and K. Susztak, "How Many Cell Types Are in the Kidney and What Do They Do?," *Annual Review of Physiology* 84 (2022): 507–531.
48. W. Wei, V. Popov, J. A. Walocha, J. Wen, and E. Bello-Reuss, "Evidence of Angiogenesis and Microvascular Regression in Autosomal-Dominant Polycystic Kidney Disease Kidneys: A Corrosion Cast Study," *Kidney International* 70 (2006): 1261–1268.
49. M. Aslam and Y. Ladilov, "Emerging Role of cAMP/AMPK Signaling," *Cells* 11 (2022): 308, <https://doi.org/10.3390/cells11020308>.
50. A. A. Kanhai, E. Sánchez-López, T. B. Kuipers, et al., "Short Salalate Administration Affects Cell Proliferation, Metabolism, and Inflammation in Polycystic Kidney Disease," *iScience* 26 (2023): 108278.
51. J. R. Wiśniewski, C. Wegler, and P. Artursson, "Subcellular Fractionation of Human Liver Reveals Limits in Global Proteomic Quantification From Isolated Fractions," *Analytical Biochemistry* 509 (2016): 82–88, <https://doi.org/10.1016/j.ab.2016.06.006>.
52. N. Pasquier, F. Jaulin, and F. Peglion, "Inverted Apicobasal Polarity in Health and Disease," *Journal of Cell Science* 137, no. 5 (2024): jcs261659, <https://doi.org/10.1242/jcs.261659>.

Supporting Information

Additional supporting information can be found online in the Supporting Information section.